Tuning mucoadhesion and mucopenetration in self-assembled poly(lactic acid)-block-poly(oligoethylene glycol methacrylate) block copolymer nanoparticles by controlling side-chain lengths

Ridhdhi Dave, Jon Mofford, Emily-Anne Hicks, Andrew Singh, Heather Sheardown*, and Todd Hoare*

Department of Chemical Engineering, McMaster University, 1280 Main St. W, Hamilton, Ontario, Canada, L8S 4L7

* To whom correspondence should be addressed

E-mail: hoaretr@mcmaster.ca, sheardow@mcmaster.ca

Abstract

The capacity to tune the degree of mucoadhesion and mucopenetration of nanoparticles is essential to improving drug bioavailability, transport, and efficacy at mucosal interfaces. Herein, self-assembled nanoparticles (NPs) fabricated from amphiphilic block copolymers of poly(lactic acid) (PLA) and poly(oligo(ethylene glycol) methacrylate) (POEGMA) with various side chain lengths (PLA-POEGMA$_n$) are reported to facilitate tunable mucosal interactions. PLA-POEGMA$_n$ nanoparticles with long PEG side chain lengths (n=20, or 40) demonstrated mucoadhesive properties based on rheological synergism, calorimetric tracking of mucin-nanoparticle interactions, and the formation of larger NP-mucin hybrid structures; in contrast, NPs fabricated from block copolymers with shorter PEG side chains (n=2/8-9 or n=8,9) showed poor mucoadhesion but penetrated through the mucin layer with significantly higher permeation rates (>80%). All NP formulations showed good cytocompatibility (viability >70%) with human corneal epithelial cells *in vitro* and no detectable acute *in vivo* ocular irritation in Sprague-Dawley rats. Coupled with the capacity of the synthetic route to easily incorporate different brush lengths and/or different functional groups into the hydrophilic block, we anticipate this approach may offer a solution in applications in which balancing mucoadhesion and mucopenetration is critical for enabling effective drug delivery.

Key words: mucoadhesion, mucopenetration, polymeric nanoparticles, mucosal delivery

Graphical abstract

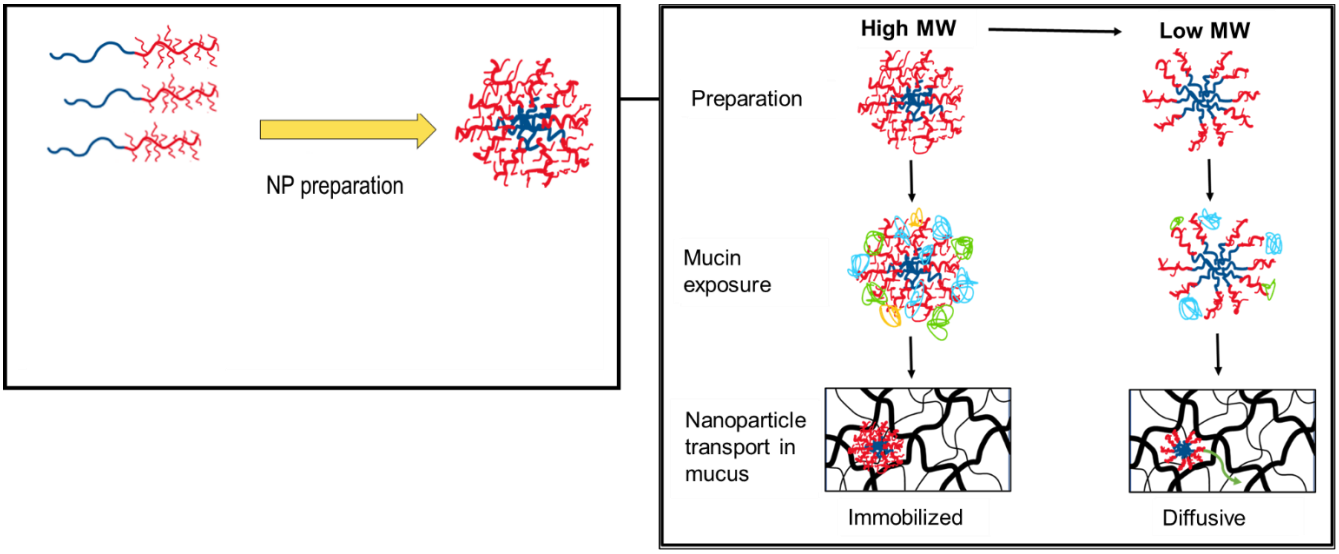

2.0 Introduction

Mucosal surfaces represent the key barrier to entry in various regions of the body such as the airway, eyes, female genitalia, and gastrointestinal tract [1]. Pathogens, toxins, and environmental fine particles can often be trapped within mucosal membranes through steric and/or adhesive interactions, thereby preventing their penetration into the body [2]. However, the same properties that help the mucus layer to protect the body from external pathogens can hinder the bioavailability and efficacy of locally delivered therapeutics to treat diseases associated with organs with mucosal membranes.

While the mucosal membrane is typically considered to be a barrier to drug delivery for the treatment of diseases that affect the mucosa, recent advances in nanomedicine and biomaterials have leveraged the mucosal membrane to improve the bioavailability of locally administered therapeutics [3]. Specifically, through the use of mucoadhesive drug delivery systems that can adhere to the mucosa (immobilizing a drug depot at the target site) or mucopenetrative drug delivery systems that can either passively or actively transport of drugs across the mucous to the underlying tissue, the efficacy and bioavailability of therapeutics can be improved [3, 4]. Many materials have been reported to promote mucin interactions through electrostatic, covalent, or physical interactions, including polysaccharides (i.e., chitosan, carboxymethyl cellulose, alginate, etc.), highly charged anionic (e.g. poly(acrylic acid)) or cationic polymers, or polymers are functionalized with thiol groups (i.e., thiomers such as chitosan-cysteine, poly(acrylic acid)-cysteamine, alginate-cysteine, etc.) or phenylboronic acid groups [3, 5, 6]. Conversely, mucosal penetration can be promoted by adding a dense layer of low-molecular weight poly(ethylene glycol) (PEG) or by incorporating high charge densities, mucolytic agents, or zeta-potential switching polymers [7].

Among PEG-based systems, self-assembled nanoparticles (NPs) based on block copolymers of PEG and poly(lactic-co-glycolic acid) (PEG-PLGA) have been demonstrated to be effective drug delivery systems to promote mucoadhesion or mucopenetration depending on the length and surface density of the PEG block [7, 8]. In terms of molecular weight, lower molecular weight PEG (< 2 kDa) minimizes mucosal adhesion based on the inherent hydrophilic and electrostatically neutral properties of PEG while higher molecular weight PEG (> 10 kDa) promotes mucosal adhesion based on physical interpenetration between the highly flexible PEG chains and the mucosal membrane and/or enhanced hydrogen bonding between the ether groups in the PEG backbone and sugars on glycosylated mucins [9]. In terms of density, NPs with low coating densities cannot shield the NP from interactions with mucus and thus promote immobilization and entrapment within the mucin layer, while NPs with high PEG densities (particularly those achievable using low molecular weight PEG) can effectively shield the NP core from mucin interactions to promote mucopenetration [7].

While linear PEG coatings have been primarily investigated in this context, changing the morphology of the PEG coating may also offer benefits for tuning NP mucoadhesion and mucopenetration. Brush, comb, or bottle-brush structures based on PEG are particularly promising given (1) their capacity to increase local PEG densities, (2) their potential to tune both the length of the polymer backbone and the length of the brushes independently, (3) their potential to mediate PEG flexibility based on the controllable steric crowding of the PEG chains, and (4) their reduced immunogenicity to counteract emerging concerns over PEG antibodies [10-12]. Such benefits have been demonstrated in other materials; for example, enhanced mucoadhesion can be achieved by creating bottle-brush polymers composed of poly(acrylic acid) grafted onto cellulose nanocrystals relative to poly(acrylic acid) alone [13]. The use of poly(oligoethylene glycol methacrylate)

(POEGMA), which is characterized by a poly(methacrylate) backbone with regular PEG side-chains, is particularly attractive in this context given that oligo(ethylene glycol) methacrylate monomers with varying PEG side chain lengths are commercially available, allowing for the production of brush-length (co)-polymers with tunable brush lengths/brush length distributions via a single-step conventional or controlled free radical polymerization [14, 15]. For example, micelles containing a poly(cholesteryl methacrylate) hydrophobic block and poly(oligo(ethylene glycol)methacrylate) (n=5-6 average side chain length) as the hydrophilic block exhibited enhanced penetration through reconstituted porcine mucus compared to those prepared with linear PEG (MW ~5000 g/mol) [16]. Similarly, wormlike nanocarriers composed of bottle-brush PEG (n=20 average side chain length) have been shown to translocate through all barriers of the airway including the mucosal membrane and become internalized within epithelial cells [17]. However, the ability to rationally tune the mucoadhesion and mucopenetration of POEGMA-coated nanoparticles by manipulating the brush length has not to the best of our knowledge previously been demonstrated.

Herein, we report the mucoadhesion and mucopenetration properties of nanoparticles prepared via the self-assembly of amphiphilic block copolymers of poly(lactic acid) (PLA) and poly(oligo(ethylene glycol) methacrylate) (POEGMA) with various side chain lengths fabricated via atom transfer radical polymerization (ATRP) [18]. We demonstrate that by tuning the length of the side chain we can optimize either mucoadhesion or mucopenetration of the self-assembled nanoparticles while also enabling easier preparation, modification, and/or functionalization of the nanoparticles based on the free radical synthesis approach in comparison to the ring opening synthetic method used for the fabrication of linear PEG-based blocks. We also demonstrate the biosafety and tissue tolerability of the self-assembled nanoparticles for ocular applications, in

which optimal tuning of mucoadhesion/mucopenetration is essential to enhance nanoparticle retention in the eye while also ensuring drug transport to the cornea.

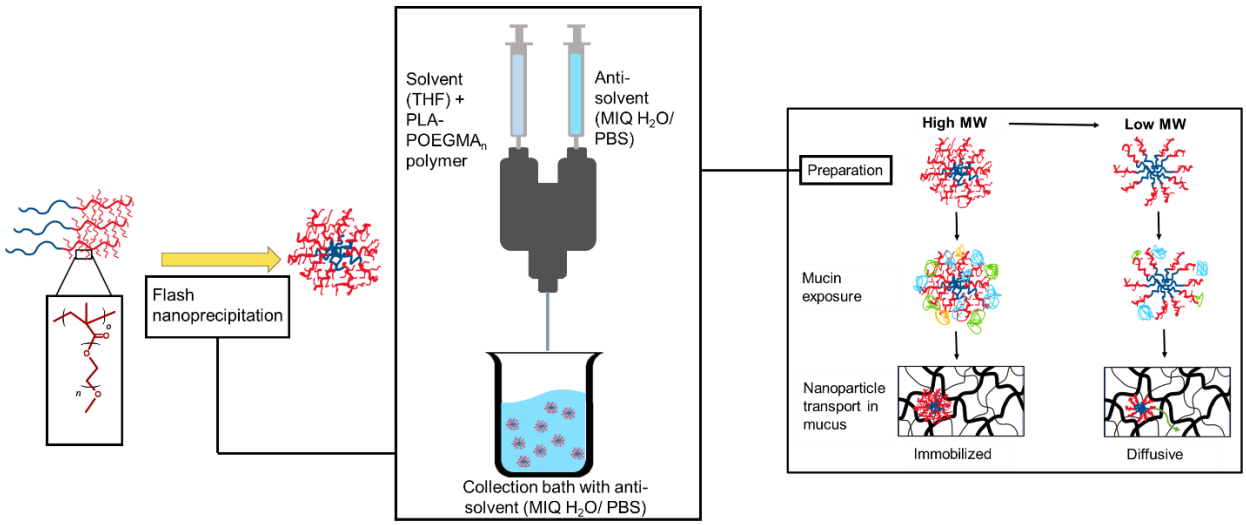

Scheme 1. Schematics of the flash nanoprecipitation process used to fabricate PLA-POEGMAn block copolymer-based nanoparticles and the differential mucin-nanoparticle interactions observed depending on the OEGMA side chain length.

3.0 Experimental Section

Materials: Oligo(ethylene glycol) methyl ether methacrylate ($OEGMA_{n=8,9}$, containing 100 ppm MEHQ 200 ppm BHT as inhibitor, 100%), di(ethylene glycol) methyl ether methacrylate ($M(EO)_2MA$, containing 100 ppm MEHQ and 200 ppm BHT as inhibitor, 95%), poly(ethylene glycol) methyl ether methacrylate ($OEGMA_{n=20}$, containing 100 ppm MEHQ and 300 ppm BHT as inhibitor, 100%), poly(ethylene glycol) methyl ether methacrylate solution ($OEGMA_{n=40}$, 50 wt. % in H_2O), 2-bromoisobutyry-terminated poly(L-lactide) (PLA-Br, 10 kDa), copper(II) bromide ($CuBr_2$, 99%), tris[2(dimethylamino)ethyl]amine (Me_6TREN, 97%), tin(II) 2-ethylhexanoate ($Sn(Oct)_2$, 92.5-100.0%), methanol (ACS reagent, ≥99.8%), tetrahydrafuran (THF,

containing 250 ppm BHT as inhibitor, ACS reagent, ≥99.0%), dichloromethane (DCM, containing 40-150 ppm amylene as stabilizer, ACS reagent, ≥99.5%), trifluoroacetic acid (TFA, ReagentPlus®, 99%), triethylamine (≥99.5%), anisole (ReagentPlus®, 99%), and pig gastric mucin (Type III) were all used as received from Sigma-Aldrich. Milli-Q water (MIQ, purified using a Millipore Simplicity System) was used for all experiments.

3.1 Polymer Synthesis

Activators regenerated by electron transfer atom transfer radical polymerization (ARGET-ATRP) were used to synthesize the PLA-POEGMA$_n$ block copolymers based on previous protocols established in our group [19]. The macroinitiator 2-bromoisobutyryl-terminated poly(L-lactide) (PLA-Br) was dissolved with OEMGA$_n$ monomer, $CuBr_2$ catalyst, and the ligand Me_6TREN in the solvent anisole (see Table 1 for full recipes for each block copolymer prepared). The mixture was degassed with argon for 45 minutes, after which $Sn(Oct)_2$ was added to the reaction mixture and the polymerization was conducted at 70°C under constant stirring. After the reaction times specified in Table 1 (chosen to ensure a constant ratio of lactic acid to ethylene oxide repeat units (LA:EO) of the POEGMA polymers between the different side chain length monomers based on previous reaction kinetics studies[20]), the polymerization was terminated by exposing the reaction mixture to oxygen and the mixture was filtered through a basic alumina column to remove $CuBr_2$ and $Sn(Oct)_2$. The resulting polymers were purified through 6 cycles of 6 hours of dialysis against methanol (SnakeSkin™ Dialysis Tubing, 10 kDa molecular weight cut-off), after which the final product was dried using a rotary evaporator and under high vacuum and stored 4°C until future use.

Table 1: List of reagents and reaction conditions for the synthesis of amphiphilic PLA-POEGMA$_n$ block copolymers with different POEGMA block side-chain lengths

Polymer	**PLA-Br (mmol)**	**OEGMA$_n$ (mmol)**	**$CuBr_2$ (mmol)**	**Me_6TREN (mmol)**	**$Sn(Oct)_2$ (mmol)**	**Anisole (mL)**	**Reaction time (min)**	**Reaction temperature (°C)**
PLA-POEGMA$_{n=2}$	0.02	3.84 (OEGMA$_{n=2}$)	0.0089	0.015	0.21	5	180	70
PLA-PO10	0.02	3.84 (OEGMA$_{n=2}$) 0.425 (OEGMA$_{n=8,9}$)	0.0089	0.015	0.21	5	150	70
PLA-POEGMA$_{n=8,9}$	0.02	2.02 (OEGMA$_{n=8,9}$)	0.0089	0.015	0.21	5	45	70
PLA-POEMGA$_{n=20}$	0.02	2 (OEGMA$_{n=20}$)	0.0089	0.015	0.21	5	30	70
PLA-POEMGA$_{n=40}$	0.02	0.95 (OEGMA$_{n=40}$)	0.0089	0.015	0.21	5	10	70

3.2 Polymer Characterization

The molecular weight of the polymer was determined by gel permeation chromatography using an Agilent 1260 Infinity II GPC operating at room temperature and a PLgel 5 μm MIXED-D 300 × 7.5 mm^2 column (Agilent Technologies). DMF containing 25 mM LiBr at a flow rate of 0.5 mL/min was used as the continuous phase and a temperature of 60 °C. DMF was chosen as the solvent given its capacity to fully solubilize both blocks of the block copolymer, while LiBr is added to inhibit polar interactions between the polymers to facilitate higher-resolution measurements. Molecular weights were reported based on a calibration performed using linear PEG standards obtained from Polymer Laboratories. The samples were filtered using a 0.2 μm nylon filter prior to analysis. The composition, LA:EO ratio, and molecular weight of the polymer was also determined through ^{1}H NMR using a Bruker 600 MHz spectrometer operating at 600 MHz and 298 K (Billerica, Massachusetts, USA). Samples were dissolved in chloroform-d_6 for analysis, with the lactic acid:ethylene oxide repeat unit ratio analyzed by comparing the peak

intensities at 5.1 ppm (the methine proton in lactic acid) and 3.8 ppm (the methylene proton in ethylene oxide).

3.3 Nanoparticle Fabrication

PLA-POEGMA$_n$ nanoparticles (NPs) were fabricated via flash nanoprecipitation using a confined impinging jet mixer (CIJM) and a pneumatic pump apparatus. One syringe containing 3 mL of a 10 mg/mL polymer solution in THF and a second syringe containing 3 mL of 10 mM PBS were respectively mounted in the two inlets of a confined impinging jet mixing device. A pneumatic pump apparatus was used to empty the full volume of the syringes into a stirred 200 mL beaker containing different volumes of MIQ or 1 mM PBS (depending on the targeted nanoparticle concentration) over three seconds. The THF was left to evaporate under constant stirring in a fume hood over a period of 24 hrs, after which the nanoparticle suspension was subsequently stored at 4°C in a 20 mL scintillation vial until further use.

3.4 Nanoparticle Characterization

3.4.1 Nanoparticle Size

The particle size was measured via dynamic light scattering using a Brookhaven 90Plus instrument running BIC Particle Solutions software (Version 2.6, Brookhaven Instruments Corporation; temperature = 25 °C). NPs were filtered through a 0.45 μm polyethersulfone filter and suspended in a 4-side clear polypropylene cuvette for analysis. Scattering was detected using a 659 nm laser configured at a 90° angle. Single nanoparticle tracking analysis (LM14 HS NanoSight Microscale, Malvern Panalytical; temperature = 25 ^{o}C, flow rate for syringe pump = 150, 100-200 particles per frame) was also used to determine NP size using a similar sample preparation process but diluting the sample to a polymer concentration of 0.1 mg/mL using MIQ H_2O prior to analysis. Morphological examination of the nanoparticles (0.1 mg/mL in MIQ H_2O) was performed using

transmission electron microscopy (JEOL 1200 EX TEMSCAM). Nanoparticles were syringe filtered through a 0.45 μm polyethersulfone filter from a 0.1 mg/mL precursor suspension and dispensed onto a Cu–Pd TEM grid, after which the sample was air-dried for 30 min. Nanoparticle size measurements from TEM images were done manually in ImageJ.

3.4.2 Nanoparticle Stability

The stability of the particles over a two-week period was analyzed by tracking the change in NP diameters and scattering count rates via dynamic light scattering (Brookhaven 90Plus Instrument running BIC Particle Solutions software). NPs were filtered through a 0.45 μm polyethersulfone prior to analysis. Scattering was detected using a 659 nm laser configured at a 90° angle at maximum intensity for the laser.

3.4.3 Nanoparticle Lower Critical Solution Temperature (LCST)

The LCST of NPs was determined using a Variant Cary 5000 UV-Visible-NIR spectrophotometer. The NPs were dissolved at a concentration of 5 mg/mL in water, placed in a quartz cuvette, and scanned at a wavelength 500 nm over a temperature range of 10-80°C, with measurements recorded at 0.5°C intervals during a temperature ramp performed at a rate of 1°C/minute. The absorbance measurements were converted to transmittance values, with the (onset) LCST identified as the temperature at which the sample transmittance fell below 95%.

3.5 Assessment of Mucoadhesion

3.5.1 Mucin solution preparation

Reconstituted mucin was prepared at the target concentration indicated for each subsequent experiment from unpurified porcine-stomach type III mucin powder by dissolving an appropriate mass of mucin in 10 mM PBS and mixing overnight. For isothermal titration calorimetry experiments, mucin solutions were prepared at 0.1 mg/mL in 10 mM PBS; for flow-through

diffusion studies, mucin solutions were prepared at 5 mg/mL in MIQ. For rheological studies, 10% wt/wt mucin solution was prepared by dissolving porcine-stomach type III mucin powder in 10 mM PBS and incubating the solution overnight at 37°C. The resulting solution was subsequently centrifuged (Beckman J2-21M/E) at 1500 × g for 30 minutes at 15°C to remove undissolved components, after which the supernatant was lyophilized to obtain the soluble fraction of mucin and stored at 4°C until further use. Solutions with targeted mucin concentrations were then generated by dissolving the soluble mucin in MIQ or a buffer solution via magnetic stirring over a 24 h period.

3.5.2 Rheological Synergism

The rheological properties of the NP suspension (5 mg/mL), mucin (10% wt/wt), and NP + mucin mixture (0.5:1 mix of NP:mucin) were assessed to quantify mucoadhesion via rheological synergism. A dynamic hybrid rheometer (Discovery HR-2, TA Instruments) operating with a 1° aluminum cone-plate geometry was used and maintained at 15°C for measurements. This lower temperature was selected to maximize hydrogen bonding interactions between the nanoparticles and mucin (the primary anticipated mechanism of mucoadhesion) and thus increase the resolution of the mucoadhesion measurements [21]. For each formulation, three different rheological experiments were performed (each in triplicate) using different samples (60 µL volume each): (1) viscosity versus shear rate sweeps; (2) strain sweeps to confirm operation within the linear viscoelastic region; and (3) frequency sweeps from 0.1 to 100 rad/s to measure the storage (G') and loss (G'') moduli. Both the shear storage modulus and the viscosity measurements were subsequently used to calculate the synergism parameter using Equation 1 (for G') or Equation 2 (for viscosity) [3]. The viscosity value used was determined at shear rate of 1 s^{-1}, while the storage modulus was determined over a frequency of 0.1-100 rad/s.

$$(\Delta G' = G'_{mixture} - (G'_{NP} + G'_{mucin}) > 0) \quad (1)$$

$$(\Delta \eta' = \eta'_{mixture} - (\eta'_{NP} + \eta'_{mucin}) > 0) \quad (2)$$

3.5.3 Isothermal titration calorimetry

Isothermal titration calorimetry (ITC) was performed using a Nano ITC low-volume system (TA Instruments). Experiments were conducted by performing 20 successive 2.5 µL injections of a 5 mg/mL nanoparticle suspension in 10 mM PBS (PLA-POEGMA$_n$ where n=2, 8-9, 20, or 40) into a cell containing 170 µL of 0.1 mg/mL isolated mucin (as per section 3.5.1) in 10 mM PBS, with all solutions degassed prior to testing. All experiments were performed at room temperature under constant stirring at 350 rpm. Titration heat signals were processed by NanoAnalyze software (TA Instruments–Waters LLC, Newcastle, DE). Data from the first injection, which is a half volume compared to the subsequent injections, was disregarded to avoid errors originating from diffusion during equilibrium of the instrument [22]. The heat of dilution associated with adding 10 mM PBS injections to the same mucin solution (without suspended nanoparticles) was used as a blank, with those measured heats of dilution subtracted from the enthalpies measured for each nanoparticle titration to enable isolation of polymer-mucin interaction heat effects.

3.6 Assessment of Mucopenetration

3.6.1 Flow-through diffusion study

Nanoparticle diffusion through a mucosal membrane was assessed using a modified Ussing chamber diffusion system (Electronic Supplementary Information (ESI) Figure S1). The donor chamber was filled with 5 mL of a 3 mg/mL suspension of nanoparticles in MIQ, while the acceptor chamber was filled with MIQ. A 0.45 µM polyethersulfone membrane (Sulfor®, Pall Corporation) was placed between the donor and acceptor chambers, and a 5 mm layer of 5 mg/mL

reconstituted mucin solution was added on top of the membrane and separated from the acceptor chamber using another 0.45 µM polyethersulfone membrane. The system was incubated for 24 h at 37°C to allow for the diffusion of the NPs through the mucin layer, after which the particle size and concentration of NPs in the acceptor chamber was measured using nanoparticle tracking analysis (LM14 HS NanoSight Microscale, Malvern Panalytical). The percent particle permeation was calculated by counting the number of particles diffusing through the mucus-coated membrane (n_C) and dividing by the number of particles that diffused through an uncoated membrane (n_U). The number of particles that diffused through the coated membrane (n_C) was normalized based on a control run using only a mucin-coated membrane with MIQ on both sides (n_M) to account for any particulate species from the mucin that may also diffuse through the membrane (Equation 3):

$$\%\ particle\ permeation = \frac{n_T - n_M}{n_U} \times 100\% \quad (3)$$

3.7 Cytotoxicity

Human corneal epithelial cells (HCECs) were cultured in keratinocyte serum-free media (KSFM) supplemented with bovine pituitary extract (0.05 mg/mL) and epidermal growth factor (0.005 mg/mL). PLA-POEGMA$_n$ NPs were prepared as described in section 3.3. The NPs were incubated overnight under UV light and then filtered through a 0.22 µm PTFE filter to ensure sterility prior to testing. HCECs were then seeded in 96-well plates at a density of 15,000 cells/well and incubated at 37°C in 5% CO_2 and 100% humidity. After 24 h, the media was replaced with 180 µL of KSFM mixed with 20 µL of PBS (material-free control), 20 µL of Triton-X (0.25% v/v) (positive control), or 20 µL of NPs to achieve final NP concentrations of 5 mg/mL, 2.5 mg/mL, 1 mg/mL, 0.5 mg/mL, 0.2 mg/mL or 0.05 mg/mL. Positive control cells were washed three times with 200 µL of sterile PBS to wash off residual Triton-X (0.25% v/v) prior to MTT testing. The plates were incubated for 4, 8, or 24 h, after which cell viability was assessed using an MTT assay

(Invitrogen) based on manufacturer's instructions (n=5). MTT media was prepared by dissolving 3-(4,5-dimethylthiazol-2-yl)-2,5-diphenyltetrazolium bromide (MTT) powder in sterile PBS at a concentration 5 mg/mL, with this MTT stock solution subsequently dissolved in 10% (v/v) media. Following removal of the incubation media from each cell well, 100 µL of MTT media was added to each plate and the plates were incubated for 3 hours, after which the supernatant was removed and the formazan crystals produced were dissolved in 200 µL of DMSO for 15 minutes. Cell viability (%) was determined by measuring the absorbance of the wells at 570 nm using a SpectraMax® ABS Plus UV-vis micro-plate reader (Molecular Devices, San Jose, California, USA), comparing the measured absorbance of treated wells (ABS_T) to the untreated (cell-only) control wells (ABS_{UT}) based on Equation (4).

$$\%Viability = \frac{ABS_T - ABS_{negative\ control}}{ABS_{UT} - ABS_{negative\ control}} \times 100\% \qquad (4)$$

3.8 *In vivo* Ocular Irritation Assay

All animal procedures were performed according to protocols approved by the Animal Research Ethics Board of McMaster University (Animal Use Protocol #19-03-11) consistent with the Animals for Research Act of Province of Ontario and the guidelines of the Canadian Council on Animal Care. NP suspensions were prepared in 10 mM PBS, purified, and sterilized as previously described, with the volume adjusted using 10 mM PBS to achieve a final concentration of 5 mg/mL. The pH of the NPs was adjusted to 7.6 to match that of the precorneal tear film [23]. A healthy Sprague-Dawley rat model (~400 g) was used to assess ocular tolerability. Prior to administration of NPs, the eyes were examined using slit lamp biomicroscopy (Phoenix Micron IV), optical coherence tomography (OCT; Phoenix Micron IV), and fluorescein staining (Alcon Fluorescein Glostrips). A volume of 20 µL of NPs (PLA-PO10, PLA-POEGMA$_{n=8,9,\ 20\ and\ 40}$) prepared at a concentration of 5 mg/mL in PBS was administered to one eye of a Sprague-Dawley

rat (n=4 per treatment) twice per day for a total of 7 days, with the other eye used as a control. Treated eyes were held shut and gently massaged for several seconds to ensure proper dispersal over the ocular surface. At the end of the test period, the treated and control eyes were re-examined using slit lamp biomicroscopy, OCT, and fluorescein staining to qualitatively assess for any abnormalities, inflammation, or material-host interactions associated with the nanoparticles. The rats were subsequently euthanized, and the eyes were harvested and fixed in formalin-acetic acid-alcohol (FAA) fixative for 24 hours and then stored in 70% ethanol prior to processing. Sagittal sections were taken in the middle of the eyes (4 μm in thickness) and stained using hematoxylin and eosin (H&E) to assess inflammatory response. Tissue samples were visualized with an Optika microscope coupled with a OptikamB3 Digital Camera, with corneal thickness measurements taken from H&E-stained slides using ImageJ software.

4.0 Results and Discussion

4.1 Polymer Synthesis and Characterization

Scheme 2 shows the general reaction scheme for the ARGET-ATRP reaction used to synthesize PLA-POEGMA$_n$ block copolymers with different POEGMA chain lengths (n=2, 8-9, 20, or 40), while Table 2 shows the final copolymer compositions and the measured molecular weights and dispersities of the polymers (see Supporting Information, Figures S2-S7 for full GPC traces). Controlled molecular weights can be achieved in the range of 20-30 kDa with relatively low dispersities (<1.4), with the significantly longer side chain n=20 and n=40 OEGMA monomers yielding higher M_n values by GPC based on the larger steric bulk of these materials that would be anticipated to lead to larger hydrodynamic diameters. ^{1}H NMR was also used to calculate molecular weight based on the known (manufacturer-supplied) molecular weight of the PLA block and the measured ratio of PLA:OEGMA residues in the purified polymer, yielding higher M_n values in the range of 30-38 kDa for all polymers; these values are likely more accurate due to the

brush structure of the PLA-POEGMA$_n$ polymers being poorly modeled by the linear PEG calibration standards used for GPC. However, regardless of the methodology used, the molecular weights of each block copolymer synthesized were similar such that molecular weight (both overall and within each block) is not a complicating variable in this work. Furthermore, the ratio between the number of lactic acid and ethylene oxide repeat units in each of the polymers tested (Table 2) is roughly equal between all the copolymers based on ^{1}H NMR analysis (see Supporting Information, Figures S8-S12 for the corresponding ^{1}H NMR spectra), enabling direct comparisons between the mucoadhesion/mucopenetration properties of the different nanoparticles based on the molecular architecture instead of the chemical composition of the block copolymers.

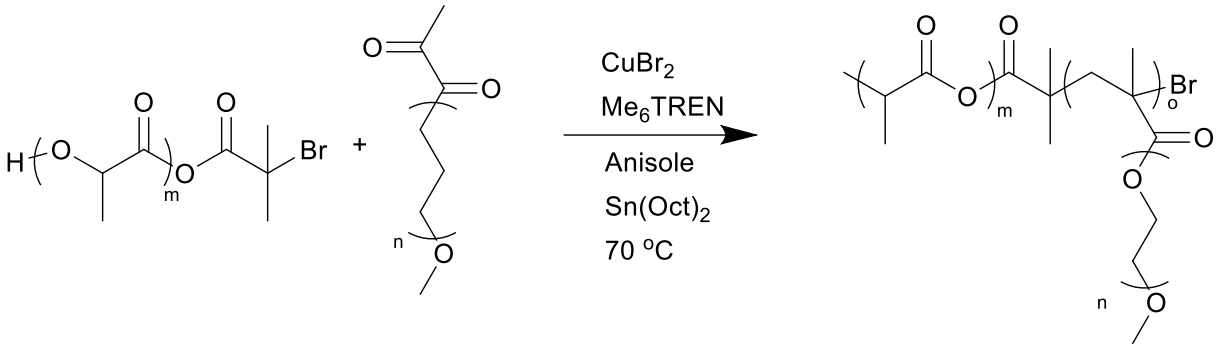

Scheme 2: Activators regenerated by electron transfer atom transfer radical polymerization reaction mechanism used to synthesize the PLA-POEGMA$_n$ block copolymers, where n is the number of average ethylene oxide repeat units in the OEGMA block (n=2, 8-9, 20 or 40), and m is the average number of lactic acid repeat units in the PLA block (m=111).

Table 2: Molecular weight, dispersity, synthesis time, and ratio between backbone repeat units (PLA:OEGMA ratio) and total repeat units (PLA:EO ratio) for PLA-POEMGA$_n$ block copolymers.

Name	#OEGMA monomer repeat units	Synthesis Time (min)	M_n (kDa) (^{1}H NMR)	M_n (kDa) (GPC)	M_w (kDa) (GPC)	Đ (GPC)	PLA:OEGMA ratio (^{1}H NMR)	PLA:EO ratio (^{1}H NMR)
PLA-PEG	-	-	-	12.0	12.4	1.04	-	-
PLA-POEGMA$_{n=2}$	2	180	37.8	18.8	25.2	1.34	111:121	111:484
PLA-PO10	4 (90 mol%) 8-9 (10 mol%)	150	33.2	23.7	24.0	1.05	111:107	111:475
PLA-POEGMA$_{n=8-9}$	8-9	45	34.7	17.5	24.7	1.41	111:52	111:438
PLA-POEGMA$_{n=20}$	20	40	32.8	32.8	39.9	1.22	111:24	111:480
PLA-POEGMA$_{n=40}$	40	15	34.0	27.3	34.1	1.25	111:12	111:458

4.2 Nanoparticle Synthesis and Characterization

NPs were fabricated using flash nanoprecipitation. Both DLS and NTA size data show that small (<100 nm) and relatively low polydispersity (0.15-0.25) nanoparticles can be produced using most of the PLA-POEGMA$_n$ copolymers (Table 3 and Figures 1A and 1B). These results are on par with or (in the case of polydispersity) somewhat lower than typical values reported for PLA-PEG block copolymers fabricated using emulsion-based methods [24-26]. Given that the pore size of the ocular mucosa is estimated to be 550±50 nm [27], the mucosal interactions of PLA-POEGMA$_n$ NPs on this length scale are not expected to be sterically hindered such that the mucoadhesive or mucopenetrative properties of the NPs will be governed by the POEGMA block morphology. The one exception to these overall trends was the significantly larger particle size measured for nanoparticles prepared with PLA-POEGMA$_{n=2}$, the shortest side chain brush copolymer that is also the least hydrophilic of the different polymers tested. We attribute this result to the near-room

temperature LCST value of this polymer, resulting in competitive hydrophobic interactions that reduce the potential of the oligo(ethylene glycol) side chains to bind water and/or sterically stabilize the nanoparticles[28]. To account for this issue while still enabling the production of a stable nanoparticle with shorter side chains, PLA-PO10 nanoparticles were fabricated in which the POEGMA block contained 90 mol% short chain (n=2 OEGMA monomer repeat units) and 10 mol% mid chain (n=8-9 OEGMA monomer repeat units) monomer; the inclusion of the small fraction of the n=8-9 OEGMA monomer increased the LCST and thus enabled the fabrication of stable <100 nm NPs with majority short chain brushes [29]. TEM (Figure 1C) indicated that all nanoparticles showed spherical morphologies similar to conventional PLA-PEG nanoparticles. Interestingly, compared with the measured particle sizes via NTA/DLS (Table 3), the particle size measured by TEM is similar for NPs prepared with linear PEG or short side chain POEGMA but becomes significantly smaller for NPs prepared with longer side chain POEGMA. We attribute this result to the high degree of surface hydration enabled by longer side chain POEGMA polymers, resulting in the hydrodynamic diameter measured by DLS/NTA being significantly higher than the dry particle diameter measured via TEM.

Table 3: Average particle size and particle size variability (as measured via dispersity for DLS and standard deviation for NTA and TEM) of PLA-POEGMA$_n$ self-assembled nanoparticles as measured by dynamic light scattering, nanoparticle tracking analysis, and transmission electron microscopy

	Dynamic Light Scattering		**Nanoparticle Tracking Analysis**		**Transmission Electron Microscopy**	
	Effective Diameter (nm)	**Đ**	**Mean Diameter (nm)**	**Standard Deviation**	**Mean Diameter (nm)**	**Standard Deviation**
PLA-PEG	162 ± 1	0.38 ± 0.02	144	67	113	85
PLA-POEGMA$_{n=2}$	217 ± 1	0.35 ± 0.04	121	61	101	75
PLA-PO10	99 ± 1	0.22 ± 0.01	88	72	50	20
PLA-POEGMA$_{n=8,9}$	56 ± 1	0.24 ± 0.01	81	47	56	32
PLA-POEGMA$_{n=20}$	80 ± 1	0.16 ± 0.01	85	45	38	20
PLA-POEGMA$_{n=40}$	82 ± 1	0.15 ± 0.02	96	44	37	15

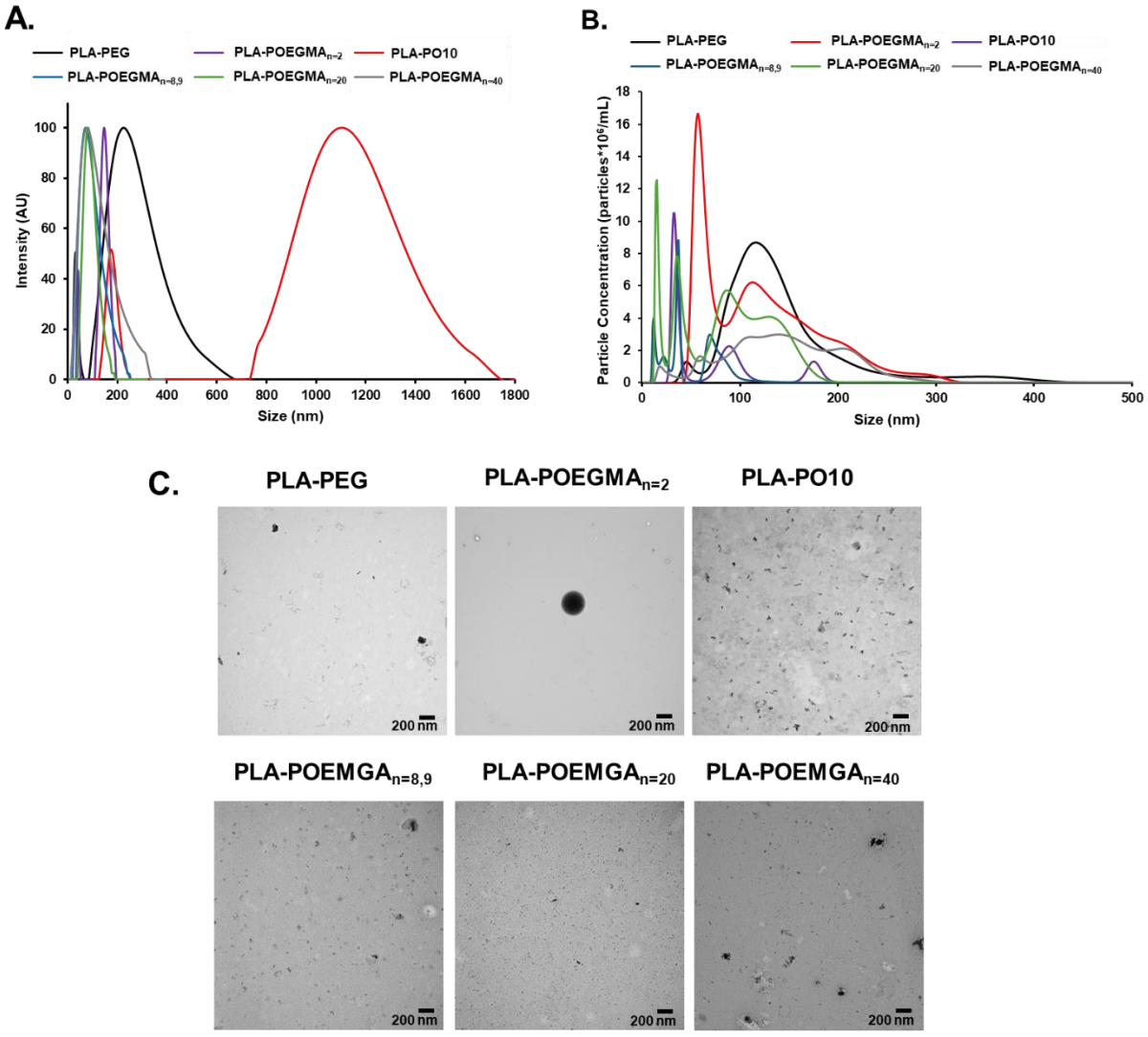

Figure 1: Size distribution of PLA-POEGMA$_n$ NPs as measured via (A) dynamic light scattering, (B) nanoparticle tracking analysis, and (C) transmission electron microscopy (50,000× magnification)

To assess the role of the LCST of the POEGMA block on controlling NP stability at the biologically relevant temperatures of 34°C at the front of the eye or 37°C in the body, the critical aggregation temperature of the NPs (which is related to the lower critical solution temperature of the POEGMA stabilizing polymers) was measured using a UV spectrophotometer (Figure 2).

Consistent with the reported linear polymer LCST values [30], PLA-POEGMA$_{n=2}$ nanoparticles showed a critical aggregation temperature of ~28°C (below the relevant physiological temperatures), PLA-PO10 shows a lower critical aggregation temperature just above physiological temperature (38°C), and PLA-POEGMA$_{n=8,9}$ (80°C), PLA-POEGMA$_{n=20}$ (85°C), and PLA-POEGMA$_{n=40}$ (89°C) all exhibited very high critical aggregation temperatures. Correspondingly, NPs prepared with OEGMA monomers with n=8,9 or larger showed consistently high colloidal stability at temperatures far above any relevant physiological condition while NPs prepared with shorter side chain lengths aggregated into larger nanostructures upon heating (Table 4); re-lowering the temperature below the LCST did not reverse the aggregation. However, apart from PLA-POEGMA$_{n=2}$ (which is thus excluded from further analysis), all nanoparticles are temperature-stable at relevant ocular conditions such that LCST behavior is not a significant contributor to the mucoadhesion/mucopenetration results to follow.

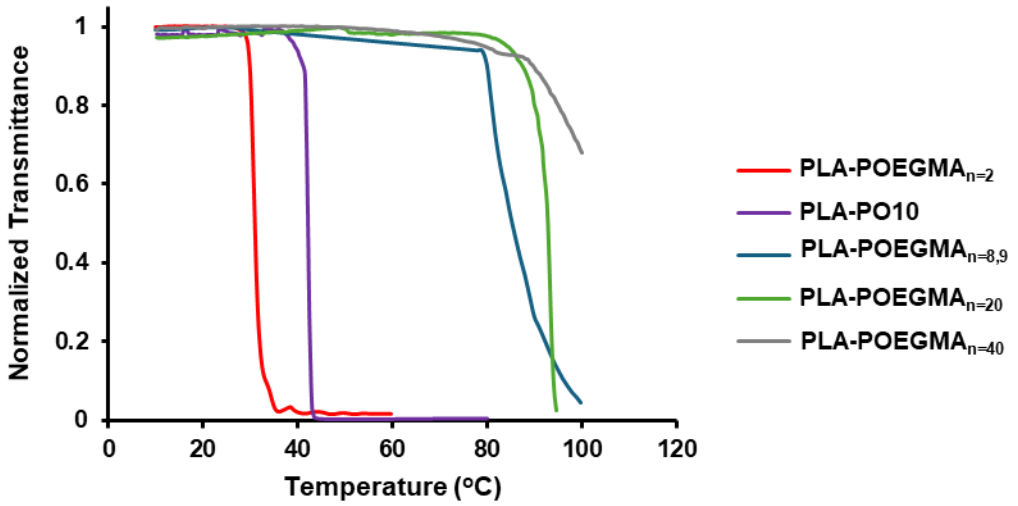

Figure 2: Critical aggregation temperature behavior of PLA-POEGMA$_n$ NPs at a concentration of 5 mg/mL in MIQ; the critical aggregation temperature is defined as the temperature at which transmittance falls below 95%.

Table 4: Critical aggregation temperature behavior of PLA-POEGMA$_n$ NPs (5 mg/mL) in MIQ

		T=25 ºC		T=LCST+5 ºC	
NP Formulation	**LCST (ºC)**	**Size (nm)**	**PDI**	**Size (nm)**	**PDI**
PLA-POEGMA$_{n=2}$	29	217 ± 1	0.15 ± 0.04	-	-
PLA-PO10	38	99 ± 1	0.22 ± 0.01	1016 ± 98	0.40 ± 0.03
PLA-POEGMA$_{n=8,9}$	80	56 ± 1	0.24 ± 0.01	626 ± 192	0.34 ± 0.01
PLA-POEGMA$_{n=20}$	85	80 ± 1	0.16 ± 0.01	222 ± 3	0.13 ± 0.02
PLA-POEGMA$_{n=40}$	89	82 ± 1	0.15 ± 0.02	172 ± 2	0.25 ± 0.02

NP stability studies were subsequently conducted to assess the potential degradation and/or aggregation of the NPs over a two-week period by measuring the change in particle size and polydispersity over time via dynamic light scattering. As shown in Figure 3, PLA-PO10, POEGMA$_{n=8-9,}$ PLA-POEGMA$_{n=20}$ and PLA-POEGMA$_{n=40}$ NPs all retained high colloidal stability over a two-week period with minimal changes in size, although the polydispersity of the PLA-POEGMA$_{n=40}$ nanoparticles increased marginally after 2 weeks suggestive of somewhat reduced colloidal stability associated the very long side chain copolymers. This result is consistent with other studies (including our own study with similar block copolymers [15]) and can be attributed the role of the longer PEG side chains in disrupting the internal packing of the PLA blocks within the mixed micelle nanoparticle core upon self-assembly, enhancing water penetration into the nanoparticle and thus accelerating nanoparticle disassembly.

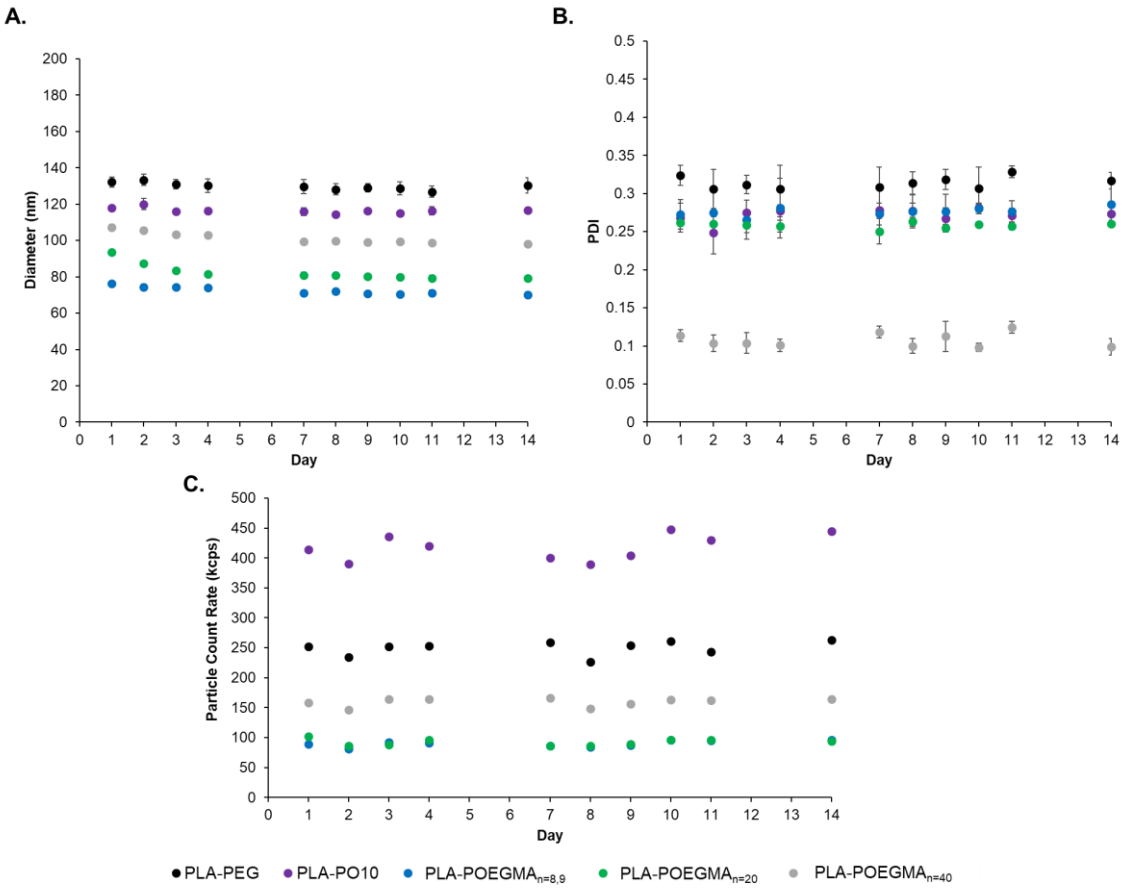

Figure 3: (A) Hydrodynamic diameter, (B) polydispersity and (C) particle count rate data from dynamic light scattering measurements for 3 mg/mL PLA-POEGMA NPs in 10 mM PBS filtered through a 0.45 mm syringe filter at 25°C following various storage times.

4.3 *In vitro* Mucoadhesion Characterization

Mucoadhesive properties were first assessed using rheological synergism experiments by comparing the storage modulus and viscosity of the nanoparticles (G'_{NP} or η_{NP}, respectively), mucin (G'_{mucin} or η_{mucin}, respectively), and the NP-mucin mixture ($G'_{mixture}$ or $\eta_{mixture}$, respectively). A mucoadhesive interaction would yield a positive synergism parameter (as defined by Equations (1) and (2)) relative to the sum of the individual storage modulus/viscosity values for mucin alone or NPs alone at the same concentrations; conversely, a mucopenetrative nanoparticle that can disrupt mucin interactions to promote mucosal transport would yield a negative or near-zero synergism parameter [3]. The synergism parameters as measured based on the shear storage modulus

plateau value and the viscosity data at a representative shear rate of 1 s^{-1} are shown in Figures 4A and 4B respectively (see Supporting Information, Figure S13 for the full viscosity vs. shear rate curves, Figure S14 for the viscosity synergism parameter vs. shear rate, and Figures S15-S18 for raw oscillatory rheology curves). Note that these studies were conducted at 15°C to enhance the elasticity of the mucin-NP complexes due to enhanced hydrogen bonding strength at lower temperature, amplifying mechanical property changes upon the application of shear to enable higher resolution measurements. Based on the shear storage modulus values, both the longer brush copolymers PLA-POEGMA$_{n=20}$ and PLA-POEGMA$_{n=40}$ showed significant larger synergism parameters than PLA-POEGMA$_{n=8,9}$, PLA-PO10, or PLA-PEG ($p < 0.05$ in pairwise comparisons); in contrast, PLA-POEGMA$_{n=8,9}$ and PLA-PO10-based NPs both showed near-zero synergism parameters. Similarly, when the synergism parameter was assessed via viscosity measurements, each of PLA-POEGMA$_{n=8,9,}$ PLA-PO10, and PLA-PEG yielded negative synergism parameters while PLA-POEGMA$_{n=20}$ and PLA-POEGMA$_{n=40}$ both showed positive synergism parameters, with significantly larger differences between the samples observed at lower shear rates consistent with the dynamic interactions between the NPs and mucin that are disrupted at higher shear (Supporting Information Figure S14). Collectively, these results suggest that the longer brush copolymers are significantly more mucoadhesive than either shorter side chain POEGMA polymers or linear PEG polymers containing the same number of ethylene oxide repeat units.

To assess the molecular-level interactions between the NPs and mucin, isothermal titration calorimetry (ITC) was applied to measure the thermodynamics of binding between mucin and nanoparticles [31]; the magnitude of the heat response can be correlated to the strength of the adhesive interaction while the sign of the heat flux values is indicative of the mechanism of the

NP-mucin interaction [32]. Figure 4C summarizes the total heat flux measured for the titration of each NP into a mucin solution for each particle (see Supporting Information, Figure S19-S22 for the raw thermograms). Consistent with the rheological synergism result, the PLA-POEGMA$_{n=20}$ and PLA-POEGMA$_{n=40}$-based particles showed much more exothermic interactions with mucin than either of the shorter side-chain analogs PLA-PO10 and PLA-POEGMA$_{n=8,9}$, suggesting that the long-chain analogues bind more strongly to mucin. Interestingly, while rheological synergism results (Figure 4A) indicated no significant difference in the mucoadhesiveness of PLA-POEGMA$_{n=20}$ and PLA-POEGMA$_{n=40}$, ITC results show that PLA-POEGMA$_{n=40}$ exhibits a significantly more exothermic interaction with mucin. We hypothesize that this observation is likely a result of the significantly higher propensity of the n=40 OEGMA polymers (in which the side chains are short polymers themselves rather than oligomers) to aggregate/reconform in solution and upon mixing with mucin, reconformations that would have their own thermodynamic signature that may partially obscure the mucoadhesion-specific binding thermodynamics.

Mucin-NP interactions were further assessed via dynamic light scattering by examining the aggregation of NPs in the presence of 0.5 mg/mL mucin over a period of 2 weeks. The change in average hydrodynamic diameter (Supporting Information Figure S24) was assessed for each NP formulation and compared to the average diameter of mucin proteins, with the change in size over the tested period reflective of NP-mucin interactions. As seen in Figure S24 and Table 5, the average size of the mucin proteins alone was maintained at ~1 μm for the duration of the test. In contrast, the average size of the NP+Mucin mixtures decreases over time, albeit to different extents depending on the side chain length; the average diameter in the PLA-PO10 and PLA-POEGMA$_{n=8,9}$ NPs + mucin mixtures decreases from ~1 μm to ~900 nm and ~800 nm, respectively, while the average diameter in PLA-POEGMA$_{n=20}$ and PLA-POEGMA$_{n=40}$ NPs +

mucin mixtures decreased from ~900 nm to ~400 nm. We hypothesize this result is indicative of the more mucoadhesive NPs bridging the mucin protein aggregates, leading to aggregation and ultimately sedimentation such that the larger particles are no longer visible in the NTA analysis (leaving only smaller particles/aggregates behind to measure). This interpretation is consistent with the changes observed in the average particle count rate over a 12 day period (Table 5), with the mucoadhesive PLA-POEGMA$_{n=20}$ and PLA-POEGMA$_{n=40}$ NPs showing a much higher reductions in the particle count rates in comparison to their non-mucoadhesive counterparts (PLA-PO10 and PLA-POEMGA$_{n=8-9}$) consistent with particle aggregation and settling over time.

Table 5: Effective diameter particle size and scattering count rates for PLA-POEGMA$_n$ nanoparticles incubated with 0.5 mg/mL mucin over a 12-day observation period as measured via dynamic light scattering

	Day 0		**Day 12**	
	Particle Size (nm)	**Count Rate (kcps)**	**Particle Size (nm)**	**Count Rate (kcps)**
0.5 mg/mL mucin	1189 ± 85	711 ± 35	719 ± 6	519 ± 16
PLA-PO10 + 0.5 mg/mL mucin	1217 ± 35	666 ± 10	783 ± 35	769 ± 10
PLA-POEGMA$_{n=8-9}$ + 0.5 mg/mL mucin	994 ± 65	769 ± 31	646 ± 11	638 ± 6
PLA-POEGMA$_{n=20}$ + 0.5 mg/mL mucin	948 ± 24	808 ± 12	360 ± 36	164 ± 1
PLA-POEGMA$_{n=40}$ + 0.5 mg/mL mucin	1131 ± 23	773 ± 15	345 ± 55	162 ± 1

4.4 *In vitro* Mucopenetration Characterization

As a complement to the mucoadhesion measurements, mucopenetration was analyzed directly via particle diffusion studies conducted using a membrane diffusion flow-through system (Figure 4D). Nanoparticles at a concentration of 3.0 mg/mL were added to the donor chamber, with their diffusion through a mucin layer (5.0 mg/mL) measured after 24 hours of incubation at 37°C using nanoparticle tracking analysis; results were normalized to account for any mucin

particulate diffusion into the acceptor chamber as measured in a separate control experiment [33]. Both PLA-PO10 and the PLA-POEGMA$_{n=8,9}$ NPs penetrate through the mucin layer with high permeation rates (>80%). In contrast, the longer side chain PLA-POEGMA$_{n=20}$ (~45% penetration) and PLA-POEGMA$_{n=40}$ (~20% penetration) nanoparticles show significantly less penetration. This result is consistent with both the mucoadhesion results (Figure 4A-C) that show significantly higher mucoadhesion associated with the longer side-chain POEGMA blocks as well as reported trends with the use of linear PEG-coated nanoparticles; for example, polystyrene nanoparticles coated with a high density of 2 kDa PEG were reported to demonstrate rapid mucosal penetration in cervical mucus while PS nanoparticles coated with 10 kDa PEG were immobilized in mucus due to their enhanced mucoadhesive potential[34].

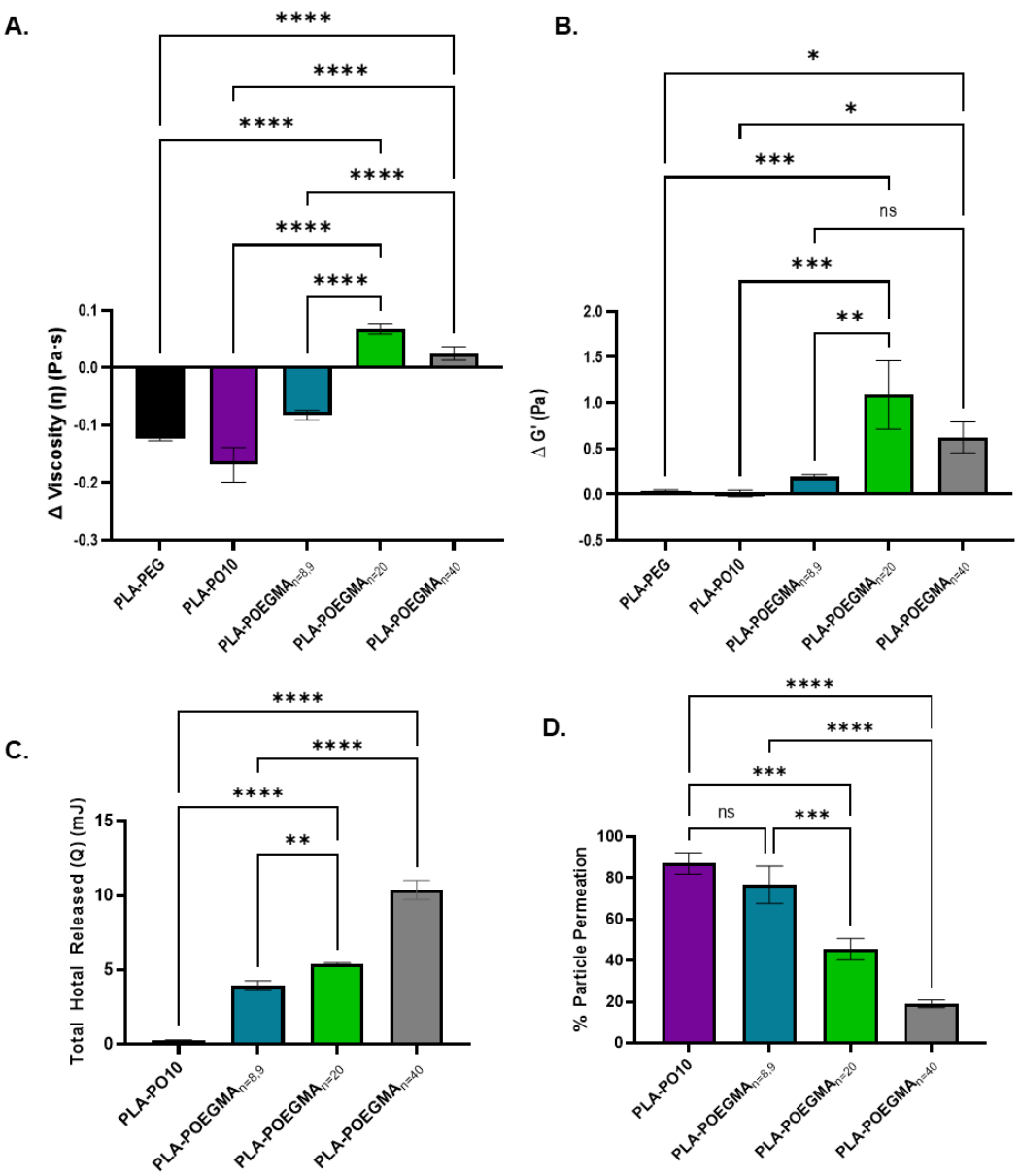

Figure 4: Mucoadhesion of PLA-POEMGA$_n$ NPs: (A,B) Rheological synergism parameters based on the measurement of (A) the shear storage modulus (G', average value over the frequency range of 0.1-10 rad/s) and (B) the viscosity (η, reported at a shear rate of 1 s^{-1}) for PLA-POEGMA$_n$ nanoparticles compared to PLA-PEG nanoparticles (10 wt/wt% mucin solution, 24 hours incubation, 15°C); (C) Total heat flux measured upon isothermal calorimetric titration of PLA-POEGMA$_n$ NPs with varying brush lengths suspended at a concentration of 5 mg/mL in 10 mM PBS into mucin (0.1 mg/mL in 10 mM PBS); heat fluxes are normalized based on heats of dilution measured by titrating a reference buffer of 10 mM PBS into the mucin solution; (D) Mucopenetration of PLA-POEGMA$_n$ NPs across a 5 mg/mL reconstituted mucus layer (thickness ~50 µm) after 24 h. Pair-wise comparison p-values: *<0.05, **<0.01, ***<0.0005, ****<0.0001.

4.5 Human corneal epithelial cell viability

To test the *in vitro* cytocompatibility of the PLA-POEGMA$_n$ nanoparticles for potential ocular applications (a key target environment for mucoadhesion/mucopenetrative materials), human corneal epithelial cells (HCECs) were incubated with PLA-POEGMA$_n$ NPs at concentrations of 50, 250, and 500 µg/mL for 24 hours and the resulting cell metabolic activity was assessed using an MTT assay relative to cell-only controls (Figure 5A). Each nanoparticle can maintain >70% cell viability at all concentrations tested consistent with the ISO standard 10993-5 for cytocompatibility; note that the higher concentrations tested herein are likely significantly greater than the effective concentration of nanoparticles on the corneal surface as a result of lachrymal drainage and rapid tear turnover *in vivo* [35]. To assess the cytocompatibility of higher concentrations of nanoparticles over shorter time frames consistent with the short residence time of tears in the eye, HCECs were also exposed to nanoparticles at concentrations of 0.5, 1, 2.5 and 5 mg/mL over shorter periods of 0.5 h (Figure 5B) and 4 h (Figure 5C). At this shorter time scale of exposure, up to 5 mg/mL NPs could still maintain high cell viabilities consistent with the cytocompatibility standard for all side chain lengths tested. Collectively, these results suggest that PLA-POEGMA$_n$ NPs are not cytotoxic to corneal epithelial cells at biologically relevant concentrations and treatment periods.

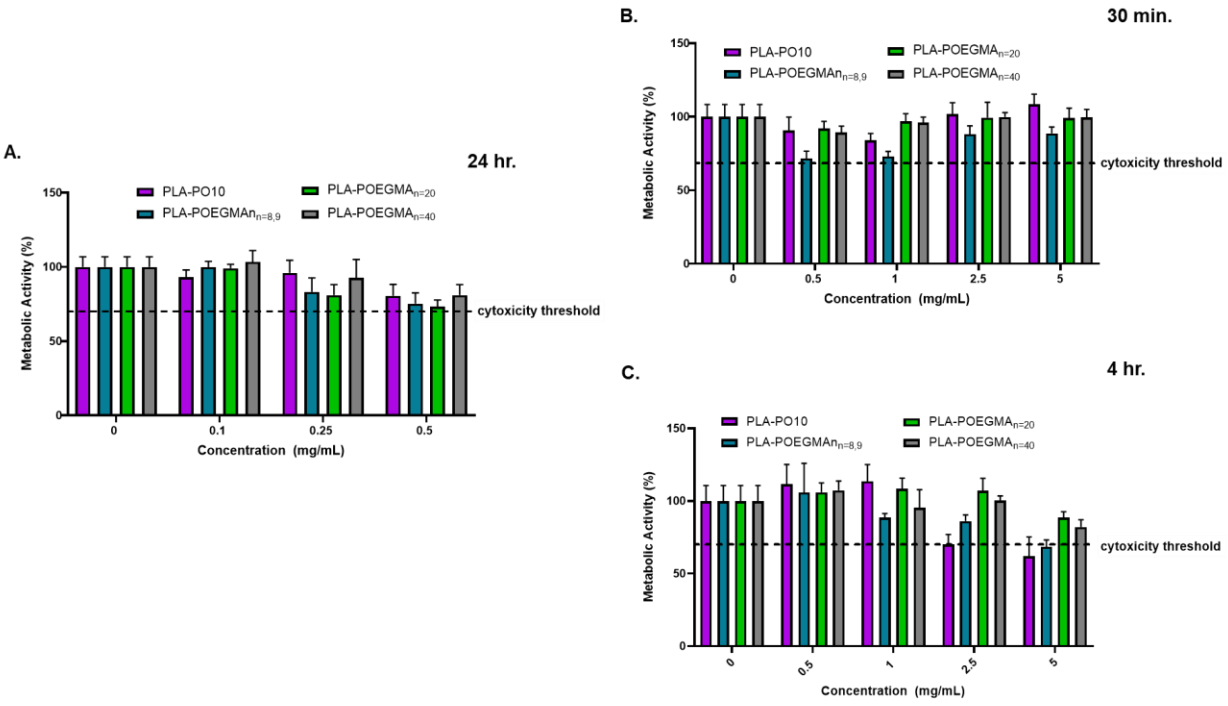

Figure 5: HCEC metabolic activity based on the MTT assay (expressed as a percentage relative to the cell-only control) for (A) cells treated with 0.1, 0.25, and 0.5 mg/mL NPs over a 24 hr period, and (B, C) cells treated with 0.5, 1, 2.5 and 5 mg/mL NPs over a period of (B) 0.5 hrs or (B) 4 hrs. The dashed line at 70% metabolic activity corresponds to the ISO 10993-5 standard for cytocompatibility.

4.6 *In vivo* ocular irritation assessment

To assess the *in vivo* tolerability of the PLA-POEGMA$_n$ nanoparticles, a 20 µL aliquot of a 5 mg/mL NP suspension was instilled as an eye drop twice daily over one week into the eye of a Sprague-Dawley rat, with the other eye used as the untreated control. The volume was chosen to scale based on surface area with a typical volumetric dose applied to human eyes, while the nanoparticle dosage was chosen to correspond to the highest short-term tolerated dose from the *in vitro* cell viability studies (Figure 5B) to maximize the degree of the irritation challenge. Following this dosing regimen, slit lamp microscopy and fluorescein staining (Figure 6A) indicated that the treated eye corneal tissue health was as good or better that of the baseline (untreated eye), with no

visible hyperemia or inflammation caused by the instillation of the NP drops. Optical coherence tomography (Figure 6B) similarly showed no significant changes in corneal thickness or composition; furthermore, the NPs themselves are not visible under microscopy, indicating they do not form aggregates on the surface of the eye.

To more quantitatively compare the corneal health of the rat eyes, the Oxford scale was used as a semi-quantitative method to score the fluorescein staining results by dividing corneal staining into six groups according to severity from 0 (absent) to 5 (severe) (Figure 6C); although this grading scheme is typically used for dry eye disease, it has been previously adapted to demonstrate corneal health to assess material-host interactions [36]. In all treatment groups, while overall scores based on fluorescein visually appeared to be lower for treated eyes when compared to baseline measurements, this result was not statistically significant (all $p>0.05$) consistent with the results from OCT and H&E staining. Similarly, no significant difference was observed in the average fluorescence intensity between the baseline and post-treatment groups as measured by ImageJ analysis ($p=0.065$ for saline, $p=0.355$ for PLA-PO10 NPs, $p=0.126$ for PLA-POEGMA$_{n=8,9}$ NPs, $p=0.219$ for PLA-POEGMA$_{n=20}$ NPs, and $p=0.071$ for PLA-POEGMA$_{n=40}$ NPs, Figure 6D). H&E staining also showed no signs of inflammation, changes in corneal thickness, or changes in the morphology within the corneal epithelial layer (Figure 6G-6I; see Supporting Information Figures S25-S29 for pictures from all animals tested). Collectively, these results confirm that the PLA-POEGMA$_n$ NPs are well-tolerated on the ocular surface.

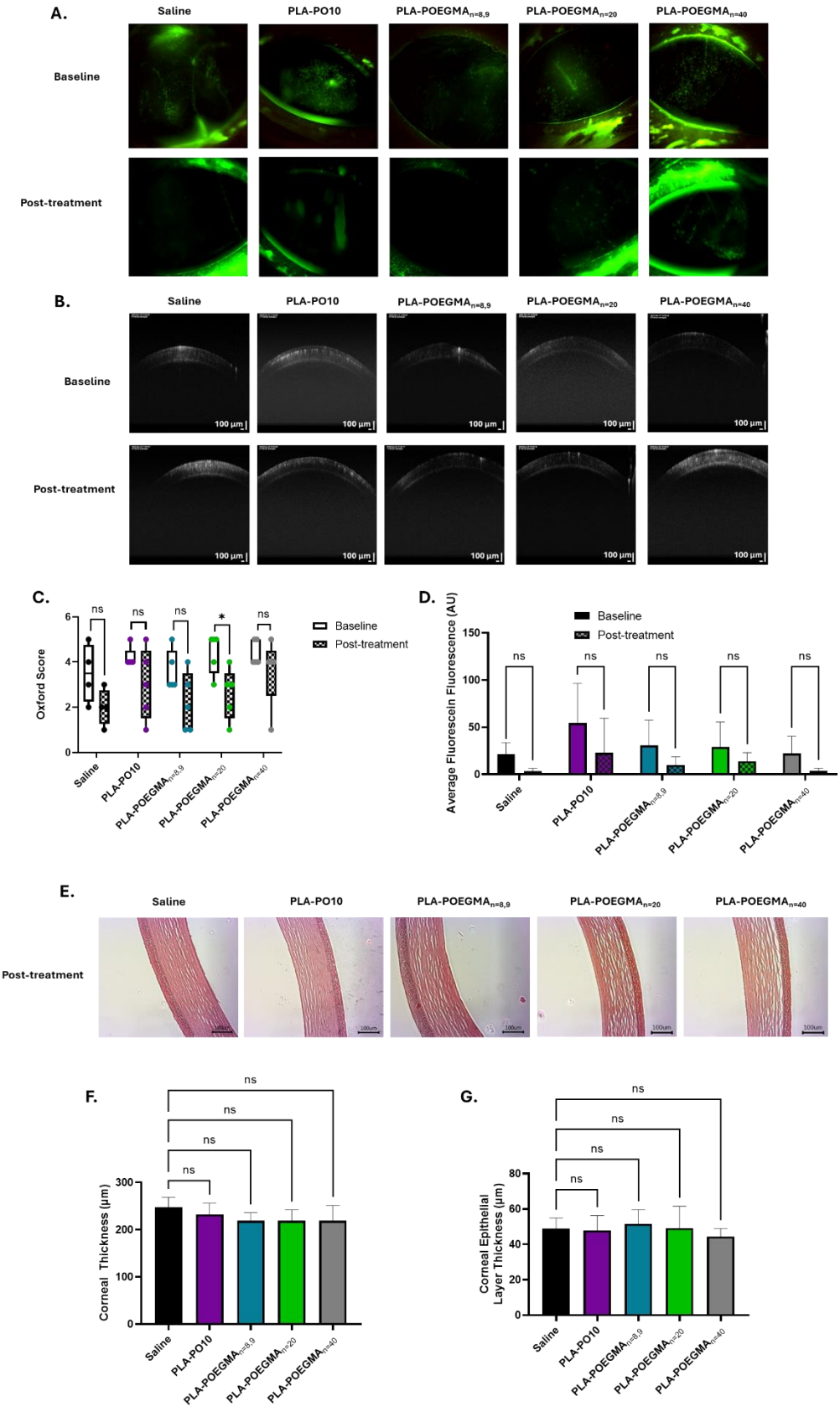
A.
Saline
PLA-PO10
PLA-POEGMA$_{n=8,9}$
PLA-POEGMA$_{n=20}$
PLA-POEGMA$_{n=40}$
Baseline
Post-treatment
B.
Saline
PLA-PO10
PLA-POEGMA$_{n=8,9}$
PLA-POEGMA$_{n=20}$
PLA-POEGMA$_{n=40}$
Baseline
Post-treatment
100 µm
C.
Oxford Score
ns
*
Baseline
Post-treatment
Saline
PLA-PO10
PLA-POEGMA$_{n=8,9}$
PLA-POEGMA$_{n=20}$
PLA-POEGMA$_{n=40}$
D.
Average Fluorescein Fluorescence (AU)
Baseline
Post-treatment
ns
Saline
PLA-PO10
PLA-POEGMA$_{n=8,9}$
PLA-POEGMA$_{n=20}$
PLA-POEGMA$_{n=40}$
E.
Saline
PLA-PO10
PLA-POEGMA$_{n=8,9}$
PLA-POEGMA$_{n=20}$
PLA-POEGMA$_{n=40}$
Post-treatment
F.
Corneal Thickness (µm)
ns
Saline
PLA-PO10
PLA-POEGMA$_{n=8,9}$
PLA-POEGMA$_{n=20}$
PLA-POEGMA$_{n=40}$
G.
Corneal Epithelial Layer Thickness (µm)
ns
Saline
PLA-PO10
PLA-POEGMA$_{n=8,9}$
PLA-POEGMA$_{n=20}$
PLA-POEGMA$_{n=40}$

Figure 6: In vivo assessment of NP safety in the eye of Sprague-Dawley rats: (A) Fluorescence images post-fluorescein staining as measured via slit-lamp microscopy to demonstrate corneal epithelial damage and (B) OCT images measured via a Spectralis OCT demonstrating changes in the corneal thickness reflective of potential scarring or epithelium damage in rat eyes treated with Cy2-labeled PLA-PO10, PLA-POEGMAn=8,9, PLA-POEGMAn=20, PLA-POEGMAn=40 NPs relative to a negative control (saline) at baseline and after twice daily instillation of 20 mL of 5 mg/mL PLA-POEGMAn NPs over a 7-day period. (C) Oxford scoring of corneal conjunctival staining of baseline (pre-treatment) and post-treatment eyes (n=5 eyes per treatment). (D) Average fluorescence from fluorescein staining before and after nanoparticle administration as measured via ImageJ image analysis (n=5 eyes per treatment). (E) H&E stained histology slices and (F,G) Overall corneal thickness (F) and corneal epithelium thickness (G) as measured from histological H&E stained slices of eyes treated with PLA-PO10, PLA-POEGMAn=8,9, PLA-POEGMAn=20, or PLA-POEGMAn=40 NPs relative to a negative control (saline) (n=5 eyes per treatment group, average taken from 3 sections of each slice).

Overall, these results demonstrate the potential of POEGMA-based hydrophilic brushes to modify the mucosal interaction properties of nanoparticles while maintaining high compatibility with the ocular surface. Relative to linear PLA-PEG polymers, the free radical polymerizability of the OEGMA-based monomers enables facile functionalization and/or mixing of OEGMA-based monomers with different chain lengths and/or different chain length gradients within the hydrophilic block, providing far more options for manipulating the hydrophilic corona around the nanoparticles without compromising synthetic simplicity. We anticipate this flexibility can be leveraged to tune the desired mucoadhesion/mucopenetration properties of the NPs suitable for different mucosal compositions and/or different therapeutic targets, not only in the ocular environment but also at other mucosal interfaces.

6. Conclusion

A platform self-assembled nanoparticle based on PLA-POEGMA amphiphilic block copolymers prepared with different side chain lengths in the POEGMA block is demonstrated to enable tunable mucoadhesive/mucopenetrative properties by tuning the length of the PEG brush on the POEGMA block. NPs fabricated from block copolymers with longer PEG side chains (PLA-POEGMA$_{n=20}$ or PLA-POEGMA$_{n=40}$) demonstrated mucoadhesive properties while NPs fabricated from block

copolymers with shorter PEG side chains (PLA-PO10 and PLA-POEGMA$_{n=8,9}$) penetrated through the mucin layer with high permeation rates (>80%). Moreover, all NP formulations showed good cytocompatibility (viability >70%) with human corneal epithelial cells *in vitro* and no detectable acute *in vivo* ocular irritation in Sprague-Dawley rats. The highly tunable nature of the POEGMA block (which enables independent tuning of the overall molecular weight, side chain length, and side chain distribution) opens new possibilities to rationally design NPs that can address clinical needs in targeting and treating diseases at mucosal sites by improving drug delivery efficiency and reducing systemic side effects.

Author contributions

Ridhdhi Dave: Conceptualization, Data curation, Formal analysis, Investigation, Methodology, Writing – original draft, **Jon Mofford:** Methodology, Investigation, **Emily-anne Hicks:** Methodology, Investigation, **Andrew Singh:** Methodology, Investigation, **Heather Sheardown:** Conceptualization, Funding acquisition, Methodology, Project administration, Resources, Supervision, Writing – review & editing, **Todd Hoare:** Conceptualization, Funding acquisition, Methodology, Project administration, Resources, Supervision, Writing – review & editing.

Conflicts of interest

There are no conflicts to declare.

Data Availability

The data supporting this article have been included as part of the Electronic Supporting Information.

Acknowledgements

The authors would like to thank Paul Gatt and Justin Bernar for the construction of the CIJ-M device. Financial support the Natural Sciences and Engineering Research Council of Canada (NSERC – Discovery Grant RGPIN-2017-06455 to TH), the NSERC CREATE Training Program for Controlled Release Leaders (ContRoL), the Ontario Research Fund (grant #RE11-049 to HS) and the Canada Research Chairs program (CRC-2020-00135 to TH) is gratefully acknowledged.

7. References

1. Kraehenbuhl, J.-P.; Neutra, M. R., Molecular and cellular basis of immune protection of mucosal surfaces. *Physiological reviews* **1992,** *72* (4), 853-879.
2. Lamm, M. E., Interaction of antigens and antibodies at mucosal surfaces. *Annual review of microbiology* **1997,** *51* (1), 311-340.
3. Dave, R. S.; Goostrey, T. C.; Ziolkowska, M.; Czerny-Holownia, S.; Hoare, T.; Sheardown, H., Ocular drug delivery to the anterior segment using nanocarriers: A mucoadhesive/mucopenetrative perspective. *Journal of Controlled Release* **2021,** *336*, 71-88.
4. Netsomboon, K.; Bernkop-Schnürch, A., Mucoadhesive vs. mucopenetrating particulate drug delivery. *European Journal of Pharmaceutics and Biopharmaceutics* **2016,** *98*, 76-89.
5. Schattling, P.; Taipaleenmäki, E.; Zhang, Y.; Städler, B., A polymer chemistry point of view on mucoadhesion and mucopenetration. *Macromolecular bioscience* **2017,** *17* (9), 1700060.
6. Muirhead, B. B.; Prosperi-Porta, G.; Sheardown, H., Phenylboronic acid based polymeric micelles for mucoadhesive anterior segment ocular drug delivery. *Invest. Ophthalmol. Vis. Sci.* **2016,** *57* (12), 2.
7. Xu, Q.; Ensign, L. M.; Boylan, N. J.; Schon, A.; Gong, X.; Yang, J. C.; Lamb, N. W.; Cai, S.; Yu, T.; Freire, E.; Hanes, J., Impact of Surface Polyethylene Glycol (PEG) Density on Biodegradable Nanoparticle Transport in Mucus ex Vivo and Distribution in Vivo. *ACS Nano* **2015,** *9* (9), 9217-27.
8. Rafat, M.; Cleroux, C. A.; Fong, W. G.; Baker, A. N.; Leonard, B. C.; O'Connor, M. D.; Tsilfidis, C., PEG-PLA microparticles for encapsulation and delivery of Tat-EGFP to retinal cells. *Biomaterials* **2010,** *31* (12), 3414-3421.
9. Maisel, K.; Reddy, M.; Xu, Q.; Chattopadhyay, S.; Cone, R.; Ensign, L. M.; Hanes, J., Nanoparticles coated with high molecular weight PEG penetrate mucus and provide uniform vaginal and colorectal distribution in vivo. *Nanomedicine* **2016,** *11* (11), 1337-1343.
10. Jia, F.; Chen, P.; Wang, D.; Sun, Y.; Ren, M.; Wang, Y.; Cao, X.; Zhang, L.; Fang, Y.; Tan, X., Bottlebrush polymer-conjugated melittin exhibits enhanced antitumor activity and better safety profile. *ACS applied materials & interfaces* **2021,** *13* (36), 42533-42542.
11. Li, Z.; Tang, M.; Liang, S.; Zhang, M.; Biesold, G. M.; He, Y.; Hao, S.-M.; Choi, W.; Liu, Y.; Peng, J., Bottlebrush polymers: From controlled synthesis, self-assembly, properties to applications. *Progress in Polymer Science* **2021,** *116*, 101387.
12. Hoang Thi, T. T.; Pilkington, E. H.; Nguyen, D. H.; Lee, J. S.; Park, K. D.; Truong, N. P., The importance of poly (ethylene glycol) alternatives for overcoming PEG immunogenicity in drug delivery and bioconjugation. *Polymers* **2020,** *12* (2), 298.
13. Vakili, M. R.; Mohammed-Saeid, W.; Aljasser, A.; Hopwood-Raja, J.; Ahvazi, B.; Hrynets, Y.; Betti, M.; Lavasanifar, A., Development of mucoadhesive hydrogels based on polyacrylic acid grafted cellulose nanocrystals for local cisplatin delivery. *Carbohydrate Polymers* **2021,** *255*, 117332.
14. Lutz, J. F.; Hoth, A., Preparation of ideal PEG analogues with a tunable thermosensitivity by controlled radical copolymerization of 2-(2-methoxyethoxy)ethyl methacrylate and oligo(ethylene glycol) methacrylate. *Macromolecules* **2006,** *39* (2), 893-896.
15. Sadowski, L. P.; Singh, A.; Luo, D. H.; Majcher, M. J.; Urosev, I.; Rothenbroker, M.; Kapishon, V.; Smeets, N. M.; Hoare, T., Functionalized poly (oligo (lactic acid) methacrylate)-block-poly (oligo (ethylene glycol) methacrylate) block copolymers: A synthetically tunable analogue to PLA-PEG for fabricating drug-loaded nanoparticles. *European Polymer Journal* **2022,** *177*, 111443.

16. Taipaleenmäki, E. M.; Mouritzen, S. A.; Schattling, P. S.; Zhang, Y.; Städler, B., Mucopenetrating micelles with a PEG corona. *Nanoscale* **2017,** *9* (46), 18438-18448.
17. He, Z. J.; Huang, B.; Cai, L. H., Bottlebrush Polyethylene Glycol Nanocarriers Translocate across Human Airway Epithelium via Molecular Architecture-Enhanced Endocytosis. *ACS Nano* **2024,** *18* (27), 17586-17599.
18. Matyjaszewski, K.; Dong, H.; Jakubowski, W.; Pietrasik, J.; Kusumo, A., Grafting from surfaces for "everyone": ARGET ATRP in the presence of air. *Langmuir* **2007,** *23* (8), 4528-4531.
19. Kwak, Y.; Matyjaszewski, K., ARGET ATRP of methyl methacrylate in the presence of nitrogen-based ligands as reducing agents. *Polymer International* **2009,** *58* (3), 242-247.
20. Singh, A.; Lofts, A.; Krishnan, R.; Campea, M.; Chen, L.; Wan, Y.; Hoare, T., The effect of comb length on the in vitro and in vivo properties of self-assembled poly (oligoethylene glycol methacrylate)-based block copolymer nanoparticles. *Nanoscale Advances* **2024,** *6* (9), 2487-2498.
21. Boddupalli, B. M.; Mohammed, Z. N.; Nath, R. A.; Banji, D., Mucoadhesive drug delivery system: An overview. *J Adv Pharm Technol Res* **2010,** *1* (4), 381-7.
22. Malvern Manual: MicroCal iTC200 system user manual (English) MAN0560. https://cmi.hms.harvard.edu/files/cmi/files/microcal-itc200-system-user-manual.pdf.
23. Tiffany, J. M., The normal tear film. *Surgery for the dry eye* **2008,** *41*, 1-20.
24. Beletsi, A.; Panagi, Z.; Avgoustakis, K., Biodistribution properties of nanoparticles based on mixtures of PLGA with PLGA–PEG diblock copolymers. *International journal of pharmaceutics* **2005,** *298* (1), 233-241.
25. Abelha, T. F.; Neumann, P. R.; Holthof, J.; Dreiss, C. A.; Alexander, C.; Green, M.; Dailey, L. A., Low molecular weight PEG–PLGA polymers provide a superior matrix for conjugated polymer nanoparticles in terms of physicochemical properties, biocompatibility and optical/photoacoustic performance. *J. Mat. Chem. B* **2019,** *7* (33), 5115-5124.
26. Mainardes, R. M.; Khalil, N. M.; Gremião, M. P. D., Intranasal delivery of zidovudine by PLA and PLA–PEG blend nanoparticles. *International Journal of Pharmaceutics* **2010,** *395* (1), 266-271.
27. Leal, J.; Smyth, H. D. C.; Ghosh, D., Physicochemical properties of mucus and their impact on transmucosal drug delivery. *Int J Pharm* **2017,** *532* (1), 555-572.
28. Lutz, J.-F., Polymerization of oligo(ethylene glycol) (meth)acrylates: Toward new generations of smart biocompatible materials. *Journal of Polymer Science Part A: Polymer Chemistry* **2008,** *46* (11), 3459-3470.
29. Lutz, J. F.; Weichenhan, K.; Akdemir, O.; Hoth, A., About the phase transitions in aqueous solutions of thermoresponsive copolymers and hydrogels based on 2-(2-methoxyethoxy)ethyl methacrylate and oligo(ethylene glycol) methacrylate. *Macromolecules* **2007,** *40* (7), 2503-2508.
30. Simpson, M. J.; Corbett, B.; Arezina, A.; Hoare, T., Narrowly Dispersed, Degradable, and Scalable Poly(oligoethylene glycol methacrylate)-Based Nanogels via Thermal Self-Assembly. *Industrial & Engineering Chemistry Research* **2018,** *57* (22), 7495-7506.
31. Freire, E.; Mayorga, O. L.; Straume, M., Isothermal titration calorimetry. *Analytical chemistry* **1990,** *62* (18), 950A-959A.
32. Stary, G.; Olive, A.; Radovic-Moreno, A. F.; Gondek, D.; Alvarez, D.; Basto, P. A.; Perro, M.; Vrbanac, V. D.; Tager, A. M.; Shi, J.; Yethon, J. A.; Farokhzad, O. C.; Langer, R.; Starnbach, M. N.; Andrian, U. H. v., A mucosal vaccine against Chlamydia trachomatis generates two waves of protective memory T cells. *Science* **2015,** *348* (6241), aaa8205.
33. Poinard, B.; Kamaluddin, S.; Tan, A. Q. Q.; Neoh, K. G.; Kah, J. C. Y., Polydopamine Coating Enhances Mucopenetration and Cell Uptake of Nanoparticles. *ACS Applied Materials & Interfaces* **2019,** *11* (5), 4777-4789.

34. Lai, S. K.; O'Hanlon, D. E.; Harrold, S.; Man, S. T.; Wang, Y.-Y.; Cone, R.; Hanes, J., Rapid transport of large polymeric nanoparticles in fresh undiluted human mucus. *Proceedings of the National Academy of Sciences* **2007,** *104* (5), 1482-1487.
35. Chaser, G.; Thassu, D., Eye Anatomy, Physiology and Ocular Barriers: Basic Considerations for Drug Delivery. *Ocular Drug Delivery Systems: Barriers and Application of Nanoparticulate Systems. Boca Raton* **2013**, 17-40.
36. Pellegrini, M.; Bernabei, F.; Moscardelli, F.; Vagge, A.; Scotto, R.; Bovone, C.; Scorcia, V.; Giannaccare, G., Assessment of corneal fluorescein staining in different dry eye subtypes using digital image analysis. *Translational vision science & technology* **2019,** *8* (6), 34-34.